AIAA 81-0634R

Sonic Fatigue Testing of an Advanced Composite Aileron

J. Soovere*
Lockheed-California Company, Burbank, Calif.

The sonic fatigue test program to verify the design of the composite inboard aileron for the L-1011 airplane is described. The composite aileron is fabricated from graphite/epoxy minisandwich covers which are attached to graphite/epoxy front spar and ribs, and to an aluminum rear spar with fasteners. The program covers the development of random fatigue data by means of coupon testing and modal studies on a representative section of the composite aileron, culminating in the accelerated sonic fatigue proof test. The composite aileron sustained nonlinear panel vibration during the proof test without failure. Viscous damping coefficients as low as 0.4% were measured on the panels. The effects of moisture conditioning and elevated temperature on the random fatigue life of both undamaged and impact damaged coupons were investigated. The combination of impact damage, moisture, and a 180°F temperature could reduce the random fatigue life by 50%.

Introduction

THE inboard aileron on the L-1011 airplane was selected as a candidate secondary airplane structure to demonstrate the cost and weight saving potential of advanced composite materials.[1] The composite aileron will be subjected, in service, to high level fanjet noise environment from the wing engines primarily during takeoff.[2] The noise environment represents one of the design conditions for the composite aileron. Consequently, a sonic fatigue program was conducted to ensure that the composite aileron would be free from sonic fatigue for the design life of the aileron.

The composite aileron could be subjected, while on the ground, to high humidity, elevated temperatures and impact damage from hail, tools, and ground handling equipment. The resulting impact damage may not always be visible on the outer surfaces. Environmental effects combined with the high noise environment could accelerate the damage growth from these impact damaged areas. As a result, a limited study of the above effects on the sonic fatigue allowables was included in the sonic fatigue program. The composite aileron could also be struck by lightning in flight. A limited investigation of the effect of lightning damage on the dynamic response of the composite aileron was included in this program. This paper presents a summary of the sonic fatigue test program for the L-1011 composite aileron, performed by the Lockheed-California Company as part of a joint program with the AVCO Aerostructures Division, sponsored by NASA.†

Composite Aileron Structure

The composite aileron structure consists of two T300/5208 graphite/epoxy tape minisandwich covers which are separated by widely spaced full-depth T300/5208 graphite/epoxy fabric ribs and a T300/5208 graphite/epoxy tape front spar. The original aluminum hinge fittings, fairings, and fairing support structures ahead of the front spar, the aluminum rear spar, and the full-depth honeycomb/glass fiber trailing-edge wedge are all retained. The minisandwich covers are constructed from two 3-ply 0.0225-in.-thick face sheets which are separated by a 0.0375-in.-thick ADX 819 syntactic (syn) core containing glass microballoons. Both covers are reinforced on the inside at the rib and spar locations, with cocured four-ply doublers consisting of three plys of graphite/epoxy tape covered with one ply of graphite/epoxy cloth. An earlier design featured only the three-ply tape doublers. The covers are attached to the ribs and spars with removable fasteners. The (45 deg, 0 deg, 135 deg, syn)$_s$ ‡ fiber orientation in the covers; the thickness of the covers, ribs, and spars; and the rib spacing were designed by loading conditions other than sonic fatigue. The wide rib spacing (Fig. 1), used in the design to reduce the number of expensive-to-manufacture ribs, is made possible by the use of the stiff minisandwich covers.

Sonic Fatigue Allowables

Coupon Tests

The details of the test procedures used to obtain the sonic fatigue allowables, in the form of random S/N (rms strain vs number of cycles) data, are given in Ref. 2. Four types of coupons were used in this program, as summarized in Table 1. Typical double cantilever coupons are illustrated in Fig. 2. The two-letter coupon series identification code, refers to the original design with the three-ply graphite/epoxy tape doubler. The same code, followed by the letter I, denotes an impact test coupon of the original design, whereas the two-letter code, followed by the letter M, denotes the modified design with a graphite/epoxy cloth doubler ply added over the three-ply tape doubler. The cloth doubler was added to provide increased grip depth for the fasteners and a more gradual transition in the cover thickness at the rib and spar locations (Fig. 3). As a consequence, an improvement in the sonic fatigue life of the modified coupons was to be expected.

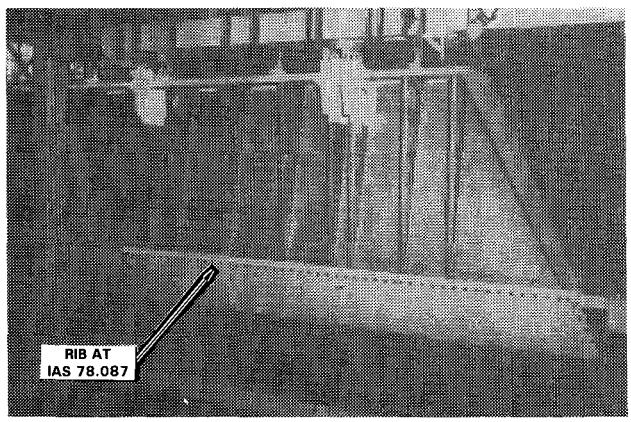

Fig. 1 L-1011 composite inboard aileron with the lower cover removed.

Presented as Paper 81-0634 at the AIAA Dynamics Specialists Conference, Atlanta, Ga., April 9-10, 1981; submitted May 13, 1981; revision received Aug. 31, 1981.

*Senior Research Specialist.

†Contract NAS 1-15069.

‡Symmetrically laminated.

Table 1 Summary of coupon configurations

COUPON SERIES	STRUCTURE SIMULATED	FIBER ORIENTATION WITH DOUBLER IF ANY	COUPON CONFIGURATION
SC	COVERS AT PANEL CENTER	$(45^0, 0^0, 135^0, SYN)_S$*	
SR	COVERS AT RIB/COVER JUNCTION	$(45^0, 0^0, 135^0, SYN, 135^0, 90^0, 45^0, 45^0, 90^0, 135^0)$	
SRM	COVERS AT RIB/COVER JUNCTION	$(45^0, 0^0, 135^0, SYN, 135^0, 0^0, 45^0, 45^0, 90^0, 135^0, 0^0_C$**$)$	
SS	COVERS AT SPAR/COVER JUNCTION	$(45^0, 90^0, 135^0, SYN, 135^0, 90^0, 45^0, 45^0, 90^0, 135^0)$	
SSM	COVERS AT SPAR/COVER JUNCTION	$(45^0, 90^0, 135^0, SYN, 135^0, 90^0, 45^0, 45^0, 90^0, 135^0, 90^0_C)$	
SRI	COVERS AT RIB/COVER JUNCTION	$(45^0, 0^0, 135^0, SYN, 135^0, 0^0, 45^0, 45^0, 90^0, 135^0)$	
RR	RIB AT RIB/COVER JUNCTION	$(45^0_C, 0^0_C, 135^0_C, 0^0_C, 45^0_C)$	

*SYMMETRICALLY LAMINATED **GRAPHITE/EPOXY CLOTH

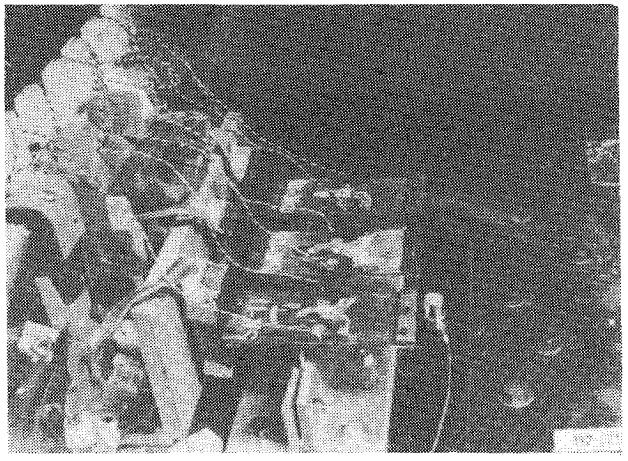

Fig. 2 Typical random fatigue coupons mounted on electromagnetic shaker in thermal enclosure—moisture conditioned SRM series coupons.

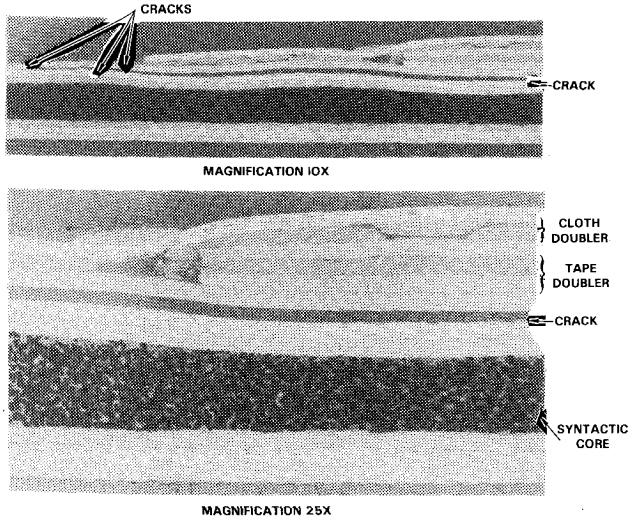

Fig. 3 Typical random fatigue cracks and core compression in SRM series coupons.

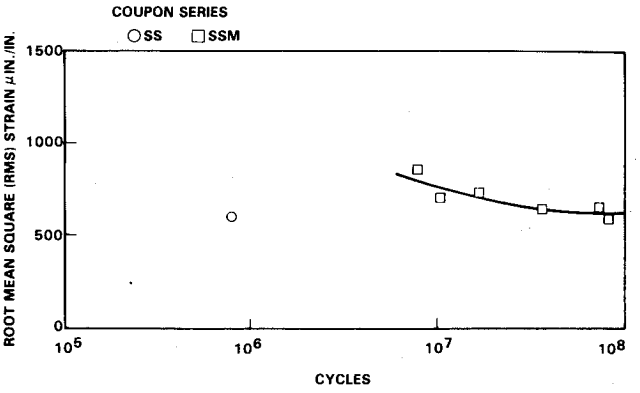

Fig. 4 Random fatigue data for the cover/spar interface.

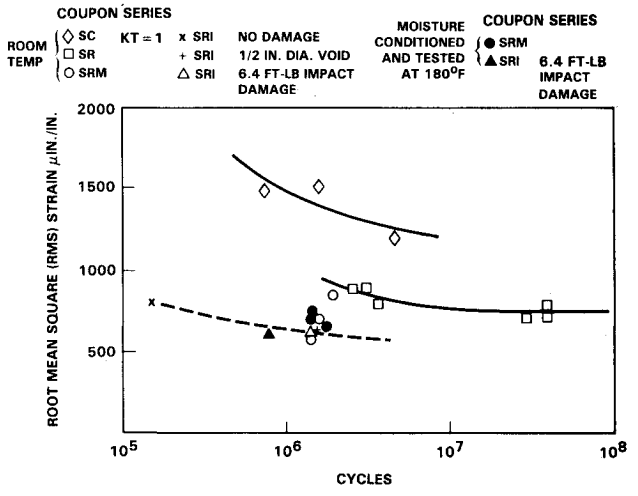

Fig. 5 Random fatigue data for the covers and the cover/rib interface.

Random Fatigue Data

The random fatigue data in Fig. 4 for the cover/spar coupons did indicate an improvement in the fatigue life. Only one series SS coupon was tested on account of the design change occurring in the middle of the coupon test program. However, the three SRM series of coupons, tested at room temperature, indicated a much lower sonic fatigue life than obtained with the SR series coupons (Fig. 5). On close inspection of the photomicrographs of sectioned SR series coupons, it was discovered that the center ply in the lower face sheet had a 90-deg fiber orientation instead of a 0-deg orientation (Table 1). Calculations indicated that, for bending at the fastener location, the combined doubler and lower face sheet stiffness is comparable to the three-ply upper face sheet stiffness. The strain levels are also comparable in the upper and lower face sheets. The more critical strain distribution around the head of the countersunk fastener is thought to be responsible for the occurrence of the failures in the upper face sheet, adjacent to the fasteners, in the SR series coupons.[2] The failure in the SSM, SRI, and the SRM series coupons were, generally, initiated in the inner skin, adjacent to the doubler edge, as illustrated in Fig. 3.

Photomicrographs of a sectioned coupon (Fig. 3) indicate that compression of the syntactic core occurred at the edges of the doublers. The reduction in the cover thickness, at the outermost doubler edge, produced a local increase in strain level which initiated the failures at that location. In the absence of syntactic core compression, there is a very strong possibility that the failures will again be initiated at the fastener locations in the upper skin. The random fatigue life will then be defined by the SR series coupon data (Fig. 5). The

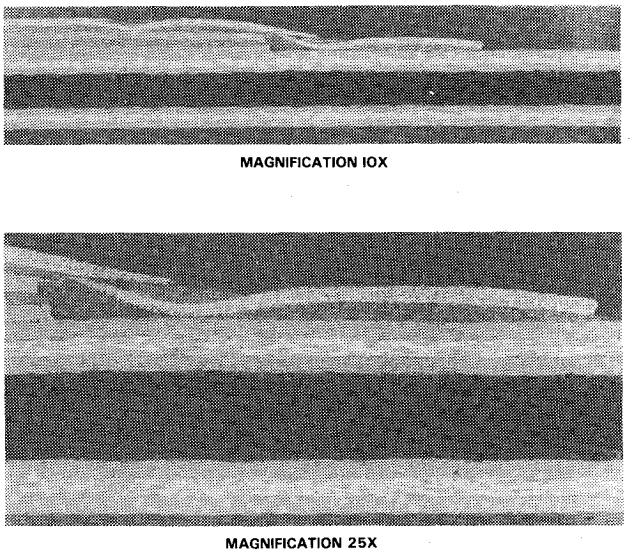

Fig. 6 Syntactic core compression eliminated by improved fabrication procedures.

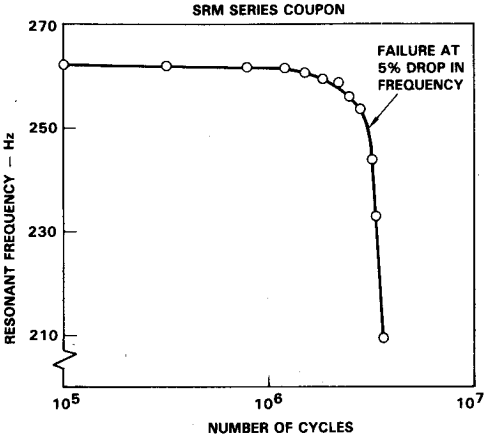

Fig. 7 Typical change in resonant frequency.

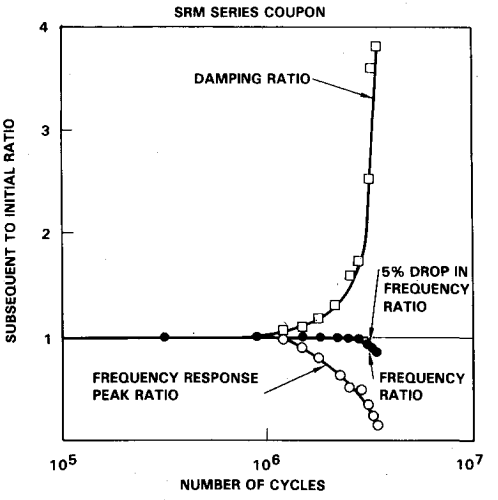

Fig. 8 Typical variation of frequency, damping, and frequency response peak ratios.

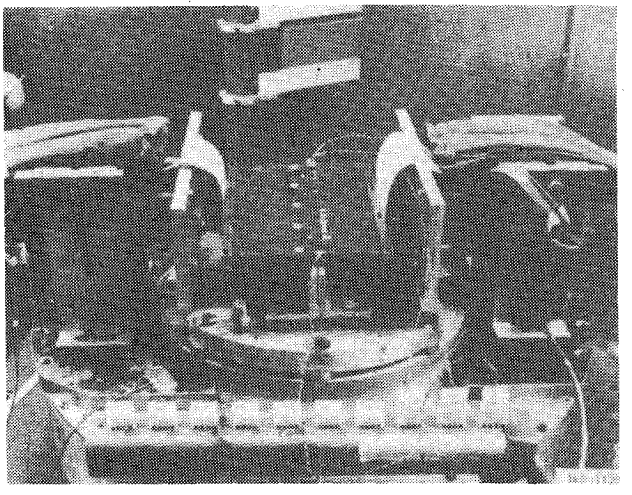

Fig. 9 Typical impact damaged coupon mounted on large electromagnetic shaker.

syntactic core compression problem has, indeed, been solved through an improved fabrication process, as seen in Fig. 6. However, no further testing was undertaken.

Effects of Moisture and Elevated Temperature

Three SRM series coupons were moisture conditioned by immersion in water at a temperature of 150°F for 19 days. These coupons were then mounted in a constant thermal enclosure on a large electromagnetic shaker (Fig. 2) and random fatigue tested at a temperature of 180°F. The excitation level was the same as for the three SRM series coupons, tested at room temperature. The test results, summarized in Fig. 5, did not indicate any degradation in sonic fatigue life due to moisture conditions and a test temperature of 180°F. The scatter in the data appears to be less in the moisture conditioned coupons.

The variation in the resonant frequency with the number of fatigue cycles, measured at the beginning of the test, during calibration, and in between each fatigue run with low level excitation,[2] is illustrated in Fig. 7 for one of the moisture conditioned coupons tested at 180°F. This resonant frequency variation is also plotted nondimensionally in Fig. 8 together with the corresponding damping and frequency response peak variations. These variations are typical for all of the SRM series coupons, but are much more pronounced than the corresponding variations for the SS and SR series coupons (see Ref. 2). As previously discussed in Ref. 2, the rapid rise in the damping can be used as an indicator of impending failure. The change in panel damping is related to the change in the delamination area. The increased damping is due to friction between the delaminated surfaces.[2]

Effect of Impact Damage

Preliminary impact tests were performed on three SRI series of coupons, illustrated in Fig. 9, to establish the impact level for visible damage. The coupons for the impact tests were simply supported along two opposite sides in a special fixture, as schematically illustrated in Fig. 10. The first coupon was subjected to multiple impacts along the rib/cover interface, at the locations and impact energy levels shown in Fig. 10. A 1-in.-diam spherically tipped rod impactor was used. Two additional coupons were tested with a smaller number of impacts to investigate the repeatability of test results. From these tests, an energy level of 6.42 ft-lb and the impact location D (Fig. 10) were selected for use in subsequent random fatigue tests. The damage was visually detectable on the inner surface. A typical impact damaged area, as detected by C-scan, is illustrated in Fig. 11.

An undamaged coupon was random fatigue tested at room temperature at a rms strain level (Fig. 5) selected from the SR series coupon fatigue test data. A very short fatigue life was obtained. Thereafter, all of the remaining three SRI series coupons were tested at a more manageable excitation level.

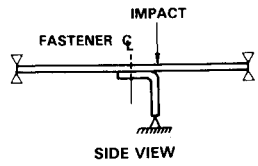

IMPACT LOCATION	ENERGY (FT-LB)	TYPE OF TEST
A	2.04	
B	6.42	
C	4.25	PRELIMINARY
D	4.25	IMPACT
E	3.15	
F	2.04	
G	6.42	
D	6.42	RANDOM FATIGUE

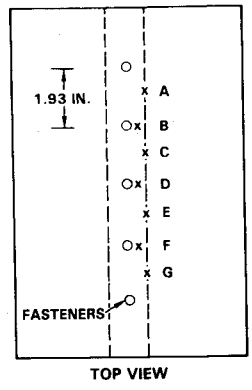

Fig. 10 Schematic of impact test setup and impact locations.

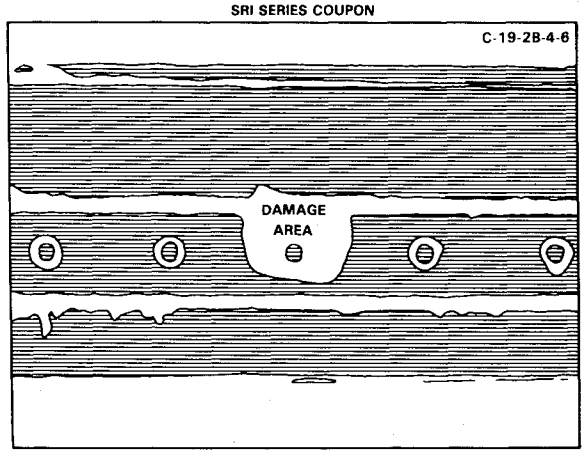

Fig. 11 Impact damaged area in moisture conditioned coupon detected by C-scan.

One of these three coupons contained a ½-in.-diam Teflon disk built into the laminate at location D (see Fig. 10). This coupon was tested at room temperature. The two remaining coupons were first impacted at location D and then tested, one at room temperature and the other, after moisture conditioning, at a temperature of 180°F. Typical damage area after random fatigue testing is illustrated in Fig. 12. The same coupon is shown in Fig. 11 before fatigue testing. Most of the damage growth occurred from the impact damaged area. However, some delaminations were initiated at the ends of the coupon.

The random fatigue data for the above coupons are summarized in Fig. 5. On the basis of the limited test data, it appears that the fatigue life is not affected by a single impact damage or the presence of a simulated void. However, the combination of a single impact damage, moisture conditioning, and a test temperature of 180°F appears to have reduced the random fatigue life by 50%. In the moisture conditioned coupon, tested at 180°F, changes in the resonant frequency, the damping, and the frequency response peak ratios were observed even at low excitation levels (Fig. 13) prior to reaching the random fatigue test level. The excitation level in all coupon tests was increased in increments up to the test excitation level for calibration purposes in case of premature strain gage failure.[2]

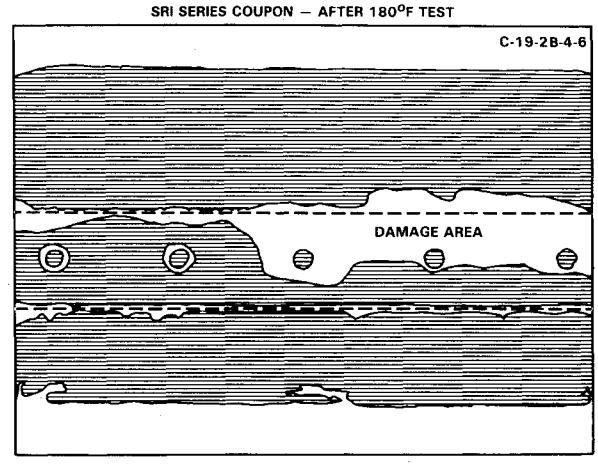

Fig. 12 Damage in moisture conditioned coupon detected by C-scan.

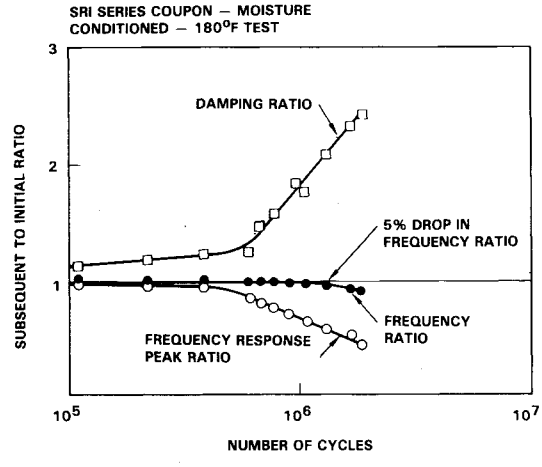

Fig. 13 Variation of resonant frequency, damping, and frequency response peak ratios.

The impact damage from multiple impacts such as those in Fig. 10 formed a continuous damage area from A to G, as indicated by C-scan, similar to the damage area in Fig. 12. Consequently, a hail storm with impact energy levels and impact densities on the ground approaching those in Fig. 10 could have serious implications for light-weight graphite/epoxy composite structures, especially if the structures are subsequently to be subjected to high-level acoustic loading. The damage at these energy levels may not be visible on the outer surface.

Sonic Fatigue Proof Test

Aileron Assembly and Mounting

The aileron assembly was required to fit into a 6-ft^2 test aperture in an acoustic progressive wave tunnel. The aileron is best attached (cantilevered) to the test frame through its hinge and actuator fittings, simulating the mounting on the airplane. Because of the dimensional restrictions, the aileron assembly between and including the hinge fitting ribs (Fig. 1) was selected. This assembly included the two largest but equal panels on either side of the rib at IAS 78-087 (Fig. 1). These panels were expected to exhibit the highest strain levels when exposed to acoustic loadings. The three-ply tape doubler configuration was used in this aileron. The aileron assembly is illustrated in Fig. 14 together with the surface strain gage locations. The remaining area within the test frame was closed out by thick plywood.

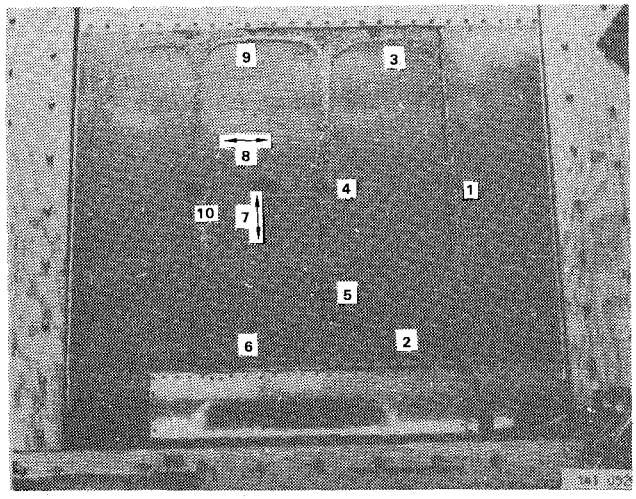

Fig. 14 Aileron assembly in test frame showing surface strain gage locations.

Table 2 Modal frequencies and dampings

Undamaged aileron		After simulated lightning strikes	
Frequency, Hz	Viscous damping coefficient	Frequency, Hz	Viscous damping coefficient
96.4	0.0042	91.18	0.0063
125.9	...	109.2	0.0038
134.3	0.0040	119.2	0.0067
149.0	0.010	126.6	0.0065
...	...	129.7	0.0091

Modal Studies

The test frame was mounted horizontally on two steel A-frames for the modal studies. Excitation was provided by means of nylon tipped impedance head hammer taps and by grazing incidence random noise from a loudspeaker. The test results[2] generally verified the conclusions reached in Ref. 3 with regard to the impedance head hammer taps vs random acoustic excitation by loudspeakers. The hammer taps tend to emphasize the antisymmetric modes involving out-of-phase motion of the two largest adjacent panels, whereas the loudspeaker excited the symmetric modes involving in-phase motion of the adjacent panels. Energy sharing between the upper and lower covers was also obtained similar to the energy sharing observed on metal control surfaces.[4] The first and second antisymmetric modes of the two large adjacent panels occurred at frequencies of 96.4 and 125.9 Hz, respectively, and the corresponding symmetric modes at 134.3 and 149 Hz, respectively. The damping coefficients for these modes are listed in Table 2. Attention is drawn to the low damping values measured on the fastener attached composite panels. A typical panel center displacement spectrum is illustrated in Fig. 15a.

Effect of Lightning Damage

The same aileron assembly, on completion of the sonic fatigue proof test, was also subjected to simulated lightning strikes and swept strokes on both the upper (Fig. 16) and the lower covers. The damage area on the lower covers involved a single lightning stroke with damage extending approximately from the number six to number seven position in Fig. 14. A limited number of hammer tap tests were performed to determine the effect of the damage on the modal frequencies

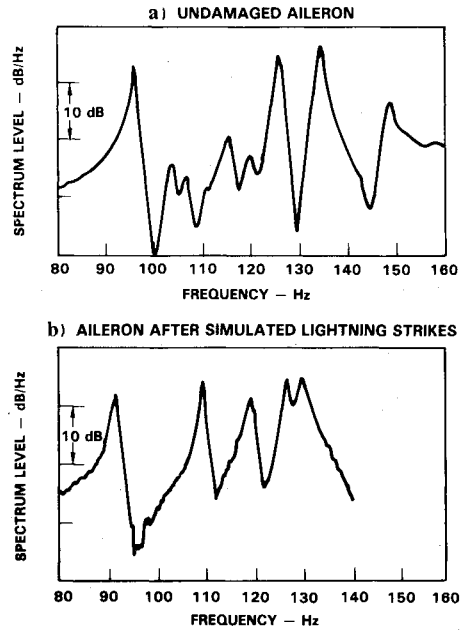

Fig. 15 Typical panel center displacement spectra.

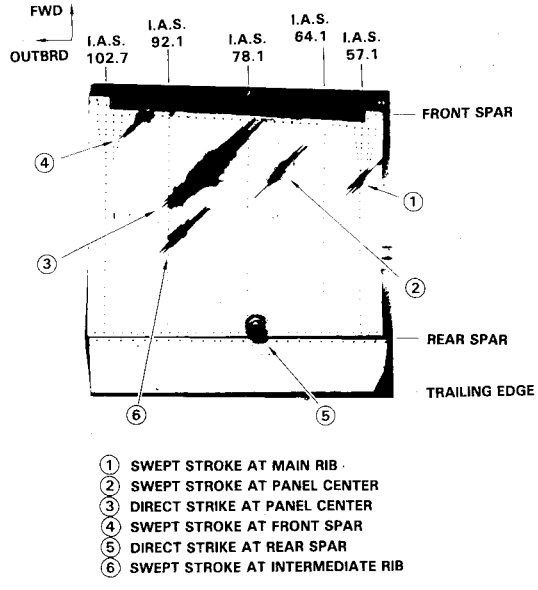

Fig. 16 Exterior of composite aileron after lightning strike tests.

and damping. The panel center response spectrum, measured between the number 7 and 8 positions in Fig. 14, is illustrated in Fig. 15b. The corresponding undamaged panel response is illustrated in Fig. 15a. As expected, all of the modes dropped in frequency by a small amount, reflecting, in view of the amount of damage sustained, the redundant nature of composite structure. However, the modal damping did not increase by as much as expected (Table 2). The reason for the small increase in damping was revealed by the C-scan. The interior laminate damage area was confined almost to the visible surface damage area. Consequently there was insufficient delamination-type crack area for generating increased damping through friction.

Proof Test

The aileron assembly was mounted in the acoustic progressive wave tunnel (PWT) (Fig. 17) for the combined calibration and panel nonlinearity test and the proof test.[2] As

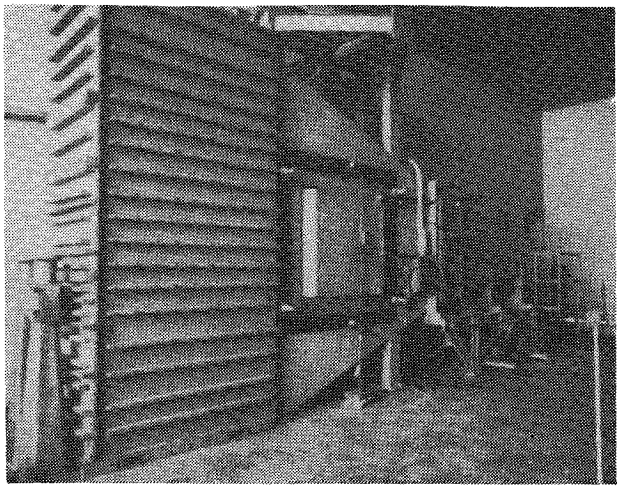

Fig. 17 Aileron assembly mounted in the acoustic progressive wave tunnel.

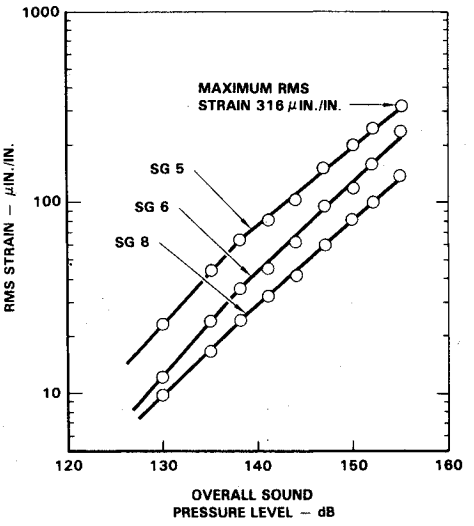

Fig. 19 Variation of rms strain with overall sound pressure level.

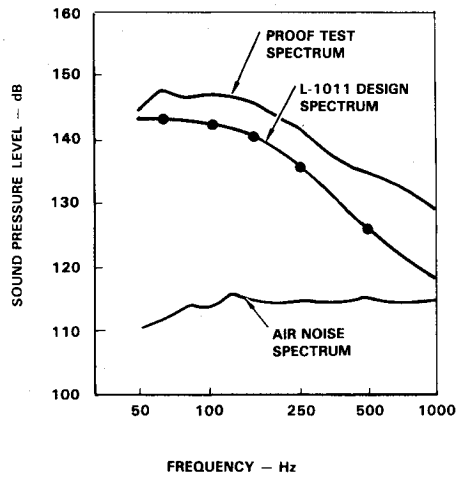

Fig. 18 Inboard aileron design, proof test, and air noise ⅓-octave band spectra.

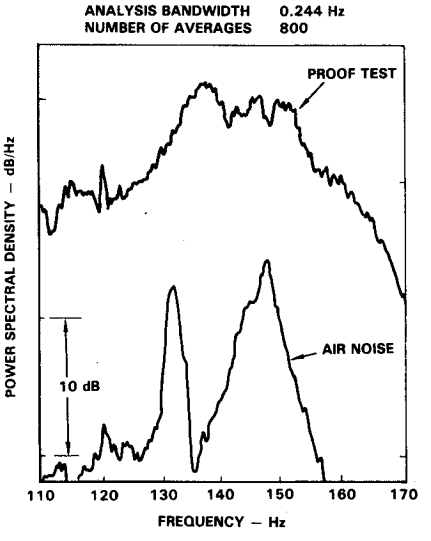

Fig. 20 Narrow-band analysis of aileron strain data—strain gage No. 5.

in the coupon tests, the strain gage outputs were calibrated against a displacement probe output in case of premature strain gage failure during the nonlinearity test. The low-level air noise spectrum, in Fig. 18, was used initially to identify the modes that are excited by the noise environment in the PWT. Thereafter, the low-level air noise was used periodically, during the nonlinearity test and the proof test, to look for frequency shifts and increases in the damping which are indicative of random fatigue failure. In the nonlinearity test, the noise level was increased, typically, in 3-dB increments up to the proof test level, which was 4.5 dB above the design noise environment (Fig. 18). An increment of only 1.5 dB was required to reduce the test time to 10 hours because of the flat profile of the random S/N curves (Figs. 4 and 5) beyond 10^7 cycles. The remaining increment was included to cover any environmental and impact damage effects and to provide a margin of safety because of the limited number of coupons used to establish the allowables.

All of the data from the ten exterior surface strain gages, the twelve interior strain gages mounted on the spars and the ribs, a reference microphone, and one displacement transducer were recorded on magnetic tape, during the nonlinearity and proof tests, for subsequent analysis. In addition, the data from three strain gages, the reference microphone, and the displacement transducer were monitored throughout the above tests and the levels measured with a rms meter having a 30-seconds averaging time. A typical plot of the rms strain data, as a function of the overall noise level at the aileron location in the PWT is illustrated in Fig. 19. The knee in the strain data in Fig. 19 indicates the presence of large-amplitude nonlinear panel response. Linear theory breaks down when the panel vibration amplitude approaches the panel thickness. An rms vibration amplitude of 0.048 in. was measured during the proof test which is close to the panel thickness of 0.0825 in. The increase in the frequencies and the broadening of the spectral peaks, observed in the proof test panel strain response spectrum in Fig. 20, is typical of nonlinear panel response. The linear strain response spectrum is included in Fig. 20 for comparison. Consequently, damping measurements obtained with the 3-dB point method, at high excitation levels, could overestimate the actual panel damping by a significant amount. For this reason the damping should be measured at low excitation levels.

No failures, frequency shifts, or increases in the damping were observed at the end of the proof test. The highest rms strain levels were measured on the covers. The strain levels measured on the ribs and the spars were generally 50% lower. The maximum rms strain level of 316 μin./in. was measured by strain gage number 5 at the rib fastener line (Fig. 14). This strain level represents a margin of approximately 6 dB for the

aileron design, based on the random fatigue allowables in Fig. 5 and approaching 9 dB, if the margin of safety built into the proof test noise level is considered. Improved fabrication procedures which eliminate the syntactic core compression problem could increase the existing margin by 2 dB.

Conclusions

The composite aileron has been shown to have a margin of safety in excess of 6 dB based on the proof test results and the random fatigue allowables obtained from the coupon tests. The damping in the fastener attached panels is very low, with values around 0.4%. Moisture conditioning and a temperature of 180°F do not appear to affect the random fatigue allowables for the composite structure. However, if impact damage is combined with moisture conditioning and the above temperature, the random fatigue life can be reduced by as much as 50%. Damage growth under these conditions is encountered at much lower excitation levels. More work is required in this area. The generally high random fatigue allowables for graphite/epoxy composites permit the panels to operate well into the nonlinear panel response region. Nonlinear analysis methods need to be developed to avoid overdesigning the structure.

References

[1] Griffin, C.F. and Fogg, L., "Design Development of an Advanced Composite Aileron," paper presented at the 5th DOD/NASA Conference on Fibrous Composites in Structural Design, New Orleans, La., Jan. 1981.

[2] Soovere, J., "Sonic Fatigue Testing of the NASA L-1011 Composite Aileron," *The Shock and Vibration Bulletin*, No. 50, Part 4, Sept. 1980, p. 13.

[3] Gordon, G.W., Wolfe, H.F., and Talmade, R.D., "Modal Investigation of Lightweight Aircraft Structures Using Digital Techniques," AFFDL-TR-124, Dec. 1977.

[4] Clarkson, B.L., "Stresses in Skin Panels Subjected to Random Acoustic Loading," AFML-TR-67-199, June 1967.